

Numerical simulation and investigation of jet impingement cooling heat transfer for the rotor blade

Amin Peiravi*, Mohsen Agha Seyyed Mirza Bozorg^a and Alireza Mostofizadeh^a

Department of Mechanical & Aerospace Engineering, Malek-Ashtar University of Technology, Isfahan, Iran

(Received June 25, 2019, Revised June 24, 2020, Accepted June 29, 2020)

Abstract. Investigation of leading edge impingement cooling for first stage rotor blades in an aero-engine turbine, its effect on rotor temperature and trailing edge wake loss have been undertaken in this study. The rotor is modeled with the nozzle for attaining a more accurate simulation. The rotor blade is hollowed in order for the coolant to move inside. Also, plenum with the 15 jet nozzles are placed in it. The plenum is fed by compressed fresh air at the rotor hub. Engine operational and real condition is exerted as boundary condition. Rotor is inspected in two states: in existence of cooling technique and non-cooling state. Three-dimensional compressible and steady solutions of RANS equations with SST $K-\omega$ turbulent model has been performed for this numerical simulation. The results show that leading edge is one of the most critical regions because of stagnation formation in those areas. Another high temperature region is rotor blade tip for existence of tip leakage in this area and jet impingement cooling can effectively cover these regions. The rotation impact of the jet velocity from hub to tip caused a tendency in coolant streamlines to move toward the rotor blade tip. In addition, by discharging used coolant air from the trailing edge and ejecting it to the turbines main flow by means of the slot in trailing edge, which could reduce the trailing edge wake loss and a total decrease in the blade cooling loss penalty.

Keywords: rotor blade; turbine cooling; jet impingement; heat transfer; CFD simulation; numerical

1. Introduction

High turbine inlet temperature is desired to achieve a lower SFC (specific fuel consumption), more efficiency, and thrust. In modern gas turbines and aero-engines the new design of the turbine's blade cooling system have been able to hold them under durable temperature and increase the turbine inlet temperature simultaneously. For existence of inertia, centrifugal and aerodynamic forces in rotor blades, addition of heat tension put them more under creep tension and hot corrosion than the other hot components of the engine. In this cooling system, high-speed air has impinged on the internal blade leading edge surface and creates a thin boundary layer on the impinged surface; particularly on the stagnation regions. Therefore, in these areas the local heat transfer coefficient is great.

Prior works on the impingement cooling shows the jet's Reynolds number, jet-hole size, the leading edge sharpness, jet to leading edge distance, jet-to-jet spacing and outflow orientation

*Corresponding author, Researcher, E-mail: amin.peiravi@gmail.com

^aProfessor, Ph.D.

which are important parameters on impingement cooling. The former parameters have been investigated by researchers in details.

Chupp *et al.* (1969) undertook an experimental investigation on the impingement cooling of the single row circular jets on the concave surface and reported the increase in heat transfer by Reynolds number amplification and a decrease in the jet leading edge distance.

Bunker and Metzger (1990) studied four different leading edge geometries which vary from sharp to semicircular leading edge with different Reynolds numbers, jet-to-jet spaces and jet to target (leading edge) distance. They found out that the overall leading edge heat transfer increases by the reduction in jet-to-jet and jet to target space and heat transfer at the leading edge increases as the geometry changes from sharp to semicircular. Dong *et al.* (2002) investigated the effect of incidence angles between the nozzles and the impingement rectangular plate on the heat transfer characteristics of pre-mixed butane/air flames with angles 90, 80, 67 and 57degrees, fixed Reynolds number and target surface distance: it was concluded that the maximum heat flux decreases as inclination angle is reduced. Ekkad *et al.* (2000) studied the effect of impingement angles ± 45 on the target surface by using liquid crystal technique for fixed Reynolds number. They noted that the orthogonal jets supply has a higher Nusselt number compared to inclined jets. Stevens and Webb (1991) examined the effect of jet inclination on local heat transfer under the obliquely impinging round free liquid jet striking at different Reynolds numbers, the angle of inclination and nozzle sizes. They concluded that an increase in inclination causes a sharpening peak in the Nusselt number profiles. Hwang and Cheng (2001) did an experimental study to measure the local heat transfer coefficient in a triangular duct which is cooled by an array of equally spaced jets aimed at the leading edge apex and exit from the radial outlet. They investigated three triangular ducts A, B, C with different apex angles 30, 45 and 60 degrees respectively for various Reynolds numbers and jet to target spacing. Results showed an increase in jet Reynolds number, an increase in heat transfer on both walls and crossflow. These effects cause a decrease in downstream local heat transfer. Tabakoff and Clevenger (1972) experimentally considered heat transfer characteristics for three different jet impingements configuration, namely a slot jet, a round jet row and array of round jets. Their results demonstrated that the slot jet with a smaller width has a better average heat transfer than the larger slot jet. It also exhibited that the round jet row has higher local heat transfer in the stagnation region while the array configurations showed more evenly distributed heat transfer. Hrycak (1981) presented heat transfer correlation for a row of impingement jets on the semicircular surface and compared the results with the experimental findings. He reported that the total heat transfer at the stagnation point of the concave surface is higher than the flat plate. Gau and Chung (1991) experimentally studied the surface curvature effects on the impingement flow structure and the heat transfer along a convex and concave surface. They attributed these results to the generation of Taylor-Görtler vortices which can increase the momentum transport in the flow and enhance the heat transfer process along the surface. Li *et al.* (2011) did a study on impingement and serpentine convection cooling under rotation conditions of turbine blades. There has been several works that have devoted to the numerical investigation of jet impingement cooling. Jia *et al.* (2002) studied slot jet impingement cooling on flat and concave surfaces with different turbulent models and compared the results with an available experimental data. Ibrahim *et al.* (2005) did a numerical simulation for jet impingements of different parameters such as jet Reynolds number, jet-to-jet plate spacing, jet diameter and target surface shape by utilizing fluent commercial code with different turbulent models. Saeed (2008) conducted a numerical simulation to survey the array of the jet impingement heat transfer on aircraft wing surfaces. He modeled a single array of jets, two stagger angles and a

case with an etched surface. Results revealed that single array and the array with a 20 degrees stagger has a better surface heat transfer than 10 degrees stagger. The etched surface yields almost 2-3 times more heat transfer than the rest.

A survey in most of the previous studies shows turbine blade complexity, like pitch and thickness variation from hub to tip, are ignored because of blade geometry simplifying. In addition only a part of the blade is investigated for impingement cooling in previous studies.

In the present study, numerical investigation is done to examine impingement cooling on leading edge of an aero-engine’s first stage rotor blade and surveying how this cooling technique can affect the heat transfer and the flow field in different regions of the rotor blade. Since this study simultaneously surveys whole turbines first stage (rotor with nozzle blades) in the existence of cooling air under the operational condition of the engine; this will provide help for designers to track all of the flow and heat transfer characteristics of this cooling technique in full.

2. Materials and methods

A three-dimensional steady turbulent flow, consisting of the nozzle, rotor blade and single row slot jets, they all have been performed in this simulation.

2.1 Geometrical details

The first stage of the turbine consists of 43 and 75 nozzle and rotor blades respectively, table 1 and 2 presents the geometrical parameters of the nozzle and the rotor at different spans. Fig.1 shows a cooled rotor blade that consists of two main parts. The first one is the plenum which is located inside of the hollowed rotor blade and 15 equal spaced rectangular jets are placed on it to spray air jets on the rotor leading edge inner surface. The jet exit width is 0.8 mm for all jets and jet-to-jet spacing is 4 times of the jet width. A hole is devised in the rotor blade’s hub to feed plenum with cooling air that has been delivered from the compressor. The second part is the main rotor blade. The plenum is located on the inside of the main rotor blade. Cooling air moves inside for an increase in heat transfer coefficient. Rotor at trailing edge is invariably slotted from hub to tip for discharging used cooling air to turbine’s main flow, as shown in Fig.1. “S” is the distance between jet holes on plenum to the leading edge and it is 2.5 times of the jet exit width; for achieving better heat transfer on the leading edge, plenum pitch is the same as the rotor pitch so jets orthogonally impinge on leading edge inner surface, Stevens and Webb (1991), Hwang and Cheng (2001).

Table 1 Nozzle parameters at different spans

	Span 0.0	Span 0.5	Span 1.0
Pitch (S^*)	19.36 mm	23.88 mm	28.39 mm
Camber Length	35.05 mm	38.22 mm	41.66 mm
Cord Length (C)	32.42 mm	35.51 mm	38.85 mm
Stagger Angle	-41.5°	-39.1°	-36.8°
Solidity (C/S^*)	1.67	1.48	1.36

Table 2 Rotor parameters at different spans

	Span 0.0	Span 0.5	Span 1.0
Pitch (S^*)	11.08 mm	13.71 mm	16.34 mm
Camber Length	28.81 mm	25.72 mm	24.45 mm
Cord Length (C)	22.94 mm	21.65 mm	21.43 mm
Stagger Angle	4.6°	14.9°	27.4°
Solidity (C/S^*)	2.07	1.57	1.31

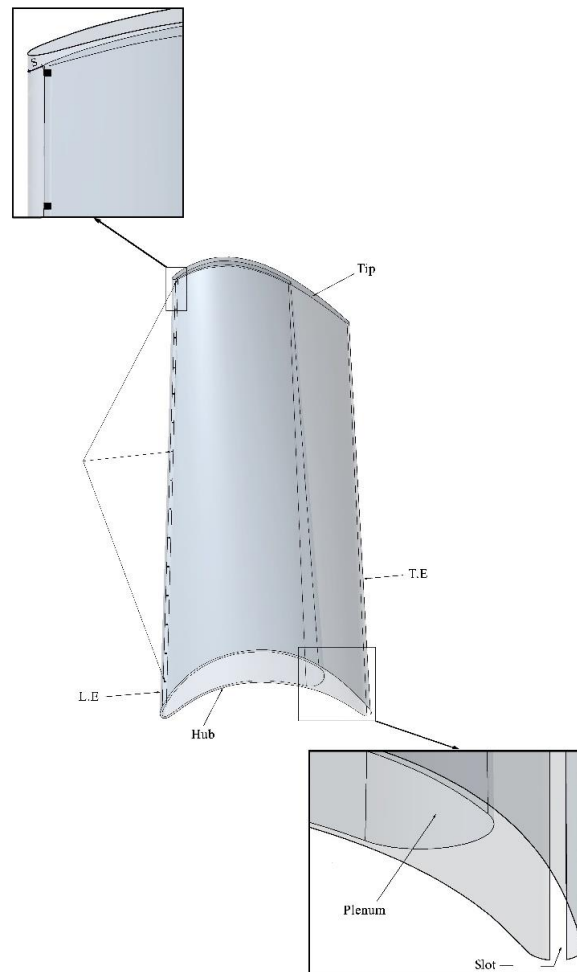


Fig. 1 Schematic of the rotor blade, plenum, jet holes and slot at the trailing edge

3. Theory/calculation

3.1 Numerical method

3.1.1 Governing equations and turbulence model

This simulation has been performed in ANSYS CFX R.17.0 commercial CFD code and the solutions have been obtained by solving the steady state and compressible Reynolds-Average Navier-Stokes equations, in which finite control volume method is adopted to discretize the equations and second order form with high-resolution correction, is applied to discretize convection term in this study. The governing equations in Cartesian tensor notation are as follows:

Continuity:

$$\frac{\partial \rho}{\partial t} + \nabla \cdot (\rho U) = 0 \quad (1)$$

Momentum:

$$\frac{\partial(\rho U)}{\partial t} + \nabla \cdot (\rho U \otimes U) = S_M - \nabla p' + \nabla \cdot \{\mu_{eff} [\nabla U + (\nabla U)^T]\} \quad (2)$$

Energy:

$$\frac{\partial(\rho h_{tot})}{\partial t} - \frac{\partial p}{\partial t} + \nabla \cdot (\rho U h_{tot}) = \nabla \cdot \left(\lambda \nabla \tau + \frac{\mu_t}{Pr_t} \nabla h \right) + \nabla \cdot (U \cdot \tau) + S_E \quad (3)$$

where U , S_M , h_{tot} , S_E , τ are the velocity component, the sum of the body forces, the total energy, the sources of energy equation, and the molecular stress tensor respectively and μ_{eff} is the effective viscosity defined by:

$$\mu_{eff} = \mu + \mu_t \quad (4)$$

where, μ_t is the eddy viscosity or turbulent viscosity and p' is modified pressure, defined by:

$$p' = p + \frac{2}{3} (\rho k + \mu_t \nabla \cdot U) \quad (5)$$

Two equations SST K- ω turbulence model have been adopted for flow prediction in this study. This model is based on eddy viscosity theory; which assumes Reynolds stress can be related to the mean velocity gradients and eddy viscosity or turbulent viscosity by gradients diffusion hypothesis. This model is recommended for high accuracy boundary layer simulation. For free shear flows, the SST K- ω model is similar to the K- ϵ model and near the solid walls, it is identical to the Wilcox's K- ω model. By this combination, SST K- ω overcomes K- ω and K- ϵ deficiencies. This switch is achieved by blending the functions of the model coefficients, Bardina *et al.* (1997).

The SST K- ω can be written as:

$$\frac{\partial(\rho k)}{\partial t} + \frac{\partial}{\partial x_j} (\rho U_j k) = P - \beta' \rho k \omega + \frac{\partial}{\partial x_j} \left[(\mu + \sigma_k \mu_t) \frac{\partial k}{\partial x_j} \right] \quad (6)$$

$$\frac{\partial(\rho \omega)}{\partial t} + \frac{\partial}{\partial x_j} (\rho U_j \omega) = \frac{\gamma}{\nu_t} P + \frac{\partial}{\partial x_j} \left[\left(\mu + \frac{\mu_t}{\sigma_{\omega 1}} \right) \frac{\partial \omega}{\partial x_j} \right] + 2(1 - F_1) \rho \sigma_{\omega 2} \frac{1}{\omega} \frac{\partial k}{\partial x_j} \frac{\partial \omega}{\partial x_j} - \beta \rho \omega^2 \quad (7)$$

$$P = \tau_{ij} \frac{\partial U_j}{\partial x_j} \quad (8)$$

See Menter (1994) for more details and origin of the parameters. The function of F_1 is applied to be one in near the wall region and zero, away from the surface. The coefficients of the model

are calculated from the coefficients ϕ_1 and ϕ_2 which represented any constant in the K- ω Wilcox model and standard K- ε model respectively.

$$\phi = F_1\phi_1 + (1 - F_1)\phi_2 \quad (9)$$

Constant related to the ϕ_1 and ϕ_2 are:

$$\beta' = 0.09, \alpha_1 = 5/9, \beta_1 = 0.075, \sigma_{k1} = 2, \sigma_{k2} = 1, \sigma_{\omega1} = 2, \sigma_{\omega2} = 1.168, \alpha_2 = 0.44, \beta_2 = 0.0828,$$

Wilcox and K- ε model overpredict the eddy-viscosity because both models do not account for the transport of the turbulent shear stress therefore, by applying a limiter to the eddy-viscosity formulation the best transport behavior can be attained as follows:

$$\nu_t = \frac{a_1 k}{\max(a_1 \omega, SF_2)} = \mu_t / \rho \quad (10)$$

where F_2 is a blending function similar to F_1 , which restricts the limiter to the wall boundary layer, S is the invariant measure of the strain rate and $a_1 = 0.31$

$$F_1 = \tanh \left(\left(\min \left(\max \left(\frac{\sqrt{k}}{\beta' \omega y}, \frac{500\nu}{y^2 \omega}, \frac{4\rho\sigma_{\omega2}k}{CD_{k\omega}y^2} \right) \right) \right)^4 \right) \quad (11)$$

$$F_2 = \tanh \left(\max \left(\frac{2\sqrt{k}}{\beta' \omega y}, \frac{500\nu}{y^2 \omega} \right)^2 \right) \quad (12)$$

where,

$$CD_{k\omega} = \max \left(2\rho\sigma_{\omega2} \frac{1}{\omega} \frac{\partial k}{\partial x_j} \frac{\partial \omega}{\partial x_j}, 1.0 \times 10^{-10} \right) \quad (13)$$

So SST K- ω now accounts for the transport of the turbulent shear stress and gives a highly accurate prediction of the onset and the amount of flow separation under adverse pressure gradients, Menter (1994).

3.2 Mesh procedure

Nozzle grid is the structured type and the unstructured grid is applied for the rotor blade. Both domain grids have been connected by general grid interface (GGI) method. When using the low Reynolds turbulence models, Y^+ less than 5 is acceptable for understanding the flow details in the boundary layer. However, Y^+ less than 2 is good and under one is excellent, Tu *et al.* (2013). In this study, Y^+ around the blades and the adjacent of the other walls (hub and shroud) is less than 2.

3.3 Grid independence analysis

For a rotor blade with or without a cooling technique case, four different meshes with different grid node numbers are shown in table 1 which are examined by SST K- ω turbulence model. In all cases Y^+ is under 2 and the rotor blade surface temperature is at a specific point, chosen as a case study. According to Table 3, the third case for non-cooling and second case for cooling the rotor blade has a good compromise between computational time and numerical accuracy. As a result,

Table 3 Nodes quantity and temperature at specific point on the rotor blade surface for the grid independence

	Non-cooling case grid node quantity	Temperature (K)	Cooling case grid node quantity	Temperature (K)
Case1	530,322	1101.1	8,213,847	1047.8
Case2	871,122	1100.9	10,663,880	1047.5
Case3	1,129,970	1099.8	12,428,817	1047.4
Case4	1,837,618	1099.8	15,327,639	1047.5

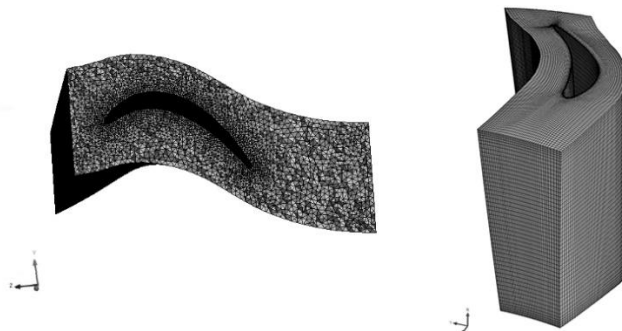


Fig. 2 Rotor (left) and nozzle mesh (right)

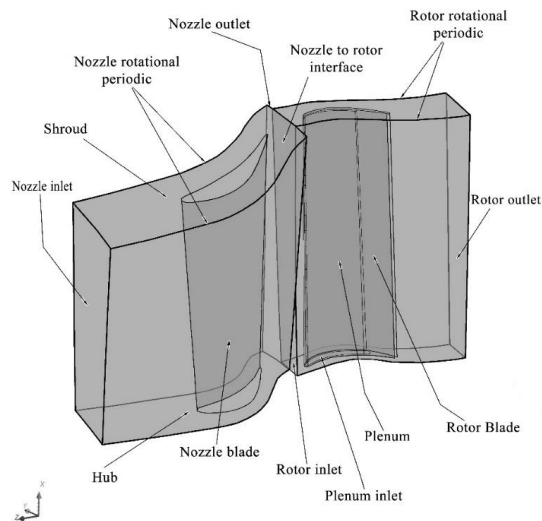


Fig. 3 Boundary condition for the nozzle and cooled rotor blade

these two case grid nodes are adopted in the present numerical simulation. Fig.2 shows nozzle and rotor blades mesh.

3.4 Boundary condition and solution procedure

Boundary condition for the cooling case is indicated in Fig. 3. Nozzle pressure and temperature inlets are 8.08 bar and 1250 K respectively. The average static pressure of the rotor outlet is 3.80

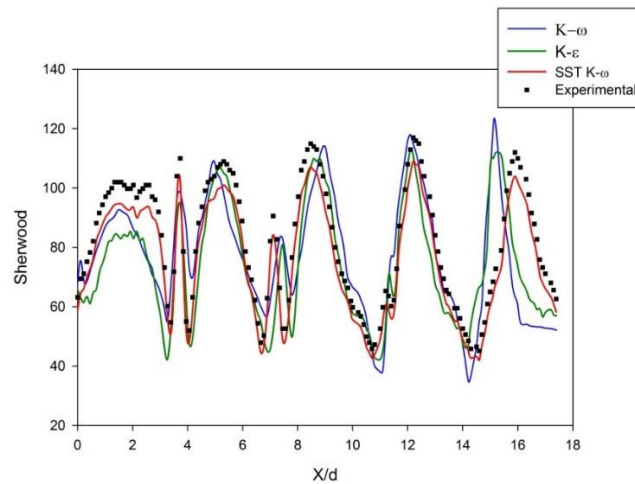


Fig. 4 Comparison between numerical and experimental local Sherwood number on concave surface along jets center line

bar. Engine's mass flow and rotational speed are 24.336 Kg/s and 16640 rpm respectively. The air ideal gas is chosen as inlet gas with $C_p = 1148 \text{ J/(Kg.K)}$ and Sutherland's formula is exerted for relating dynamic viscosity to temperature. Tip clearance is considered 0.5% of the rotor span length and cooling air boundary condition is a mass flow inlet which 0.5% of compressor's airflow (0.5% of 24.336 Kg/s) with the temperature of 675K deliver to 75 rotor blades and enters the rotor from plenum inlet at the blade's hub to feeds cooling jets. Nozzle's domain has been connected to the rotor's domain by an interface boundary condition.

3.5 Comparisons with available experimental data

For validating the capability of different turbulence models in order to explain the flow details and heat transfer in the current study, an experimental investigation which has been performed by Hong *et al.* (2008) is used as model verification. The impingement cooling in the rotating duct is selected as a case study. Computations are done with three different turbulent models, K- ϵ model, K- ω model and SST K- ω model and the values of Sherwood spanwise length at centerline is compared with the experimental data. Sherwood and the Nusselt numbers are analogous and they are equal in study by Goldstein and Cho (1995). Although K- ϵ model exhibited a good prediction of flow and heat/mass transfer behavior compared to the K- ω model in this study, SST K- ω was the best model with the maximum relative error of 14.0% for this reason, SST K- ω model is exerted in the current study. Geometrical details and operating conditions are available in Hong *et al.* (2008).

4. Results and discussions

4.1 Surveying temperature distribution in non-cooling condition

Inspection of contours and the charts for temperature distribution show that there are two main

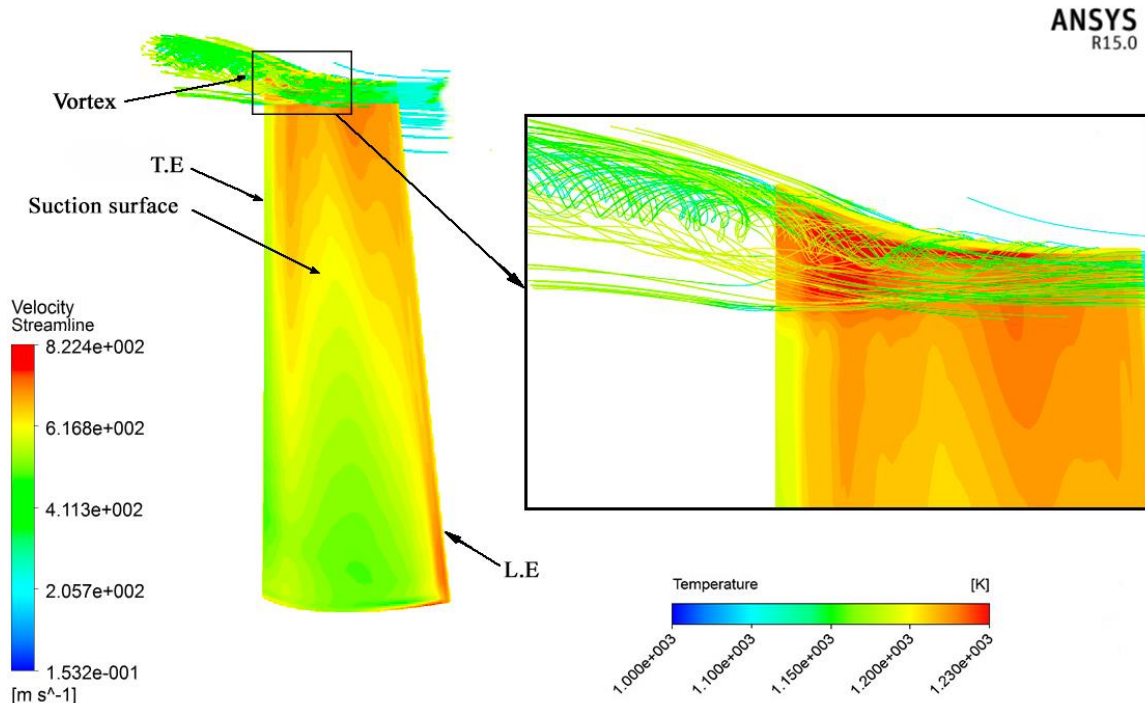


Fig. 5 Generated vortex on suction surface

critical regions in the rotor blade. One is the leading edge from hub to tip which due to the formation of stagnation point, heat transfer is considerable on this area and parameters such as free shear turbulence intensity, unsteady wakes, surface roughness and geometry impress on heat transfer in this region, Froessling (1958). Another thermal stress is near the midspan length towards the blade tip on the suction surface. These thermal stresses are more considerable on the blade tip due to the existence of tip clearance vortices which are induced by pressure differences at the blade tip. Fig.5 shows temperature distribution on the rotor blade surface in existence of streamlines. As it shows, these vortices have started from the leading edge on the pressure side and have continued to the trailing edge towards the suction side. As they move from the leading edge to the trailing edge they become larger and embrace more of the rotor blade’s surface area. These vortices consist of high main flow gas temperatures and cause severe flow mixing and turbulence. This increases the heat transfer at the suction side of the rotor blade’s tip, Metzger and Rued (1989). T_{max} on the rotor blade surface is 1230K.

4.2 Surveying temperature distribution in non-cooling condition

Blockage at the end of plenum increases the static pressure. In addition, rotation cause Coriolis forces ($2\vec{\omega} \times \vec{v}_r$) and centrifugal forces ($\vec{\omega} \times \vec{\omega} \times \vec{r}$), which both have a direct effect on the momentum equation and cause radial pressure gradient in plenum, Greitzer *et al.* (2007). Thus jet speed increase at the end of the plenum ($V_{max}=265.2$ m/s), Fig. 6 shows jets velocity profile at the center of the jet holes plate; location 0.0 is nearest to hub and 1.0 is nearest to tip.

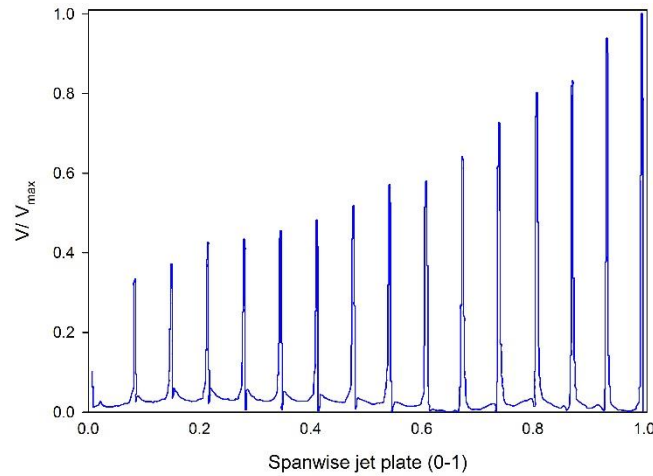


Fig. 6 Jet velocity profiles at the center plane of jets

Table 4 Jets' Reynolds number (1 is the nearest jet to the hub)

Jet No.	Reynolds Number
1	2420
2	2501
3	2715
4	2767
5	2881
6	3013
7	3169
8	3350
9	3385
10	3514
11	3807
12	4095
13	4196
14	4531
15	4723

Fig. 7 shows the temperature contour on the rotor blade suction and the pressure surface in existence of impingement cooling. Fig. 8 shows the temperature distribution at 30%, 50%, 70%, 80% and 90% of rotor blade span in cooling and no cooling condition which T_{max} is the nozzle's inlet temperature (1250 K). As observed, in non-cooling condition, moving towards the blade tip the temperature increases. Subsequently, in the existence of impingement cooling the temperature decreases. Firstly, the reason for this phenomenon is the increase in jets momentum. As they reach towards the blade tip, the high-speed flow raises the local and the average heat transfer near the tip. Another reason is the mixture of flows that are between the free spaces of the plenum and the

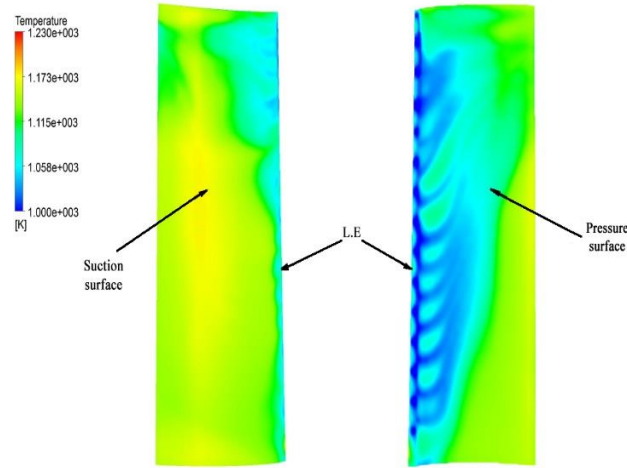


Fig. 7 Temperature distribution on suction and pressure surface in existence of impingement cooling

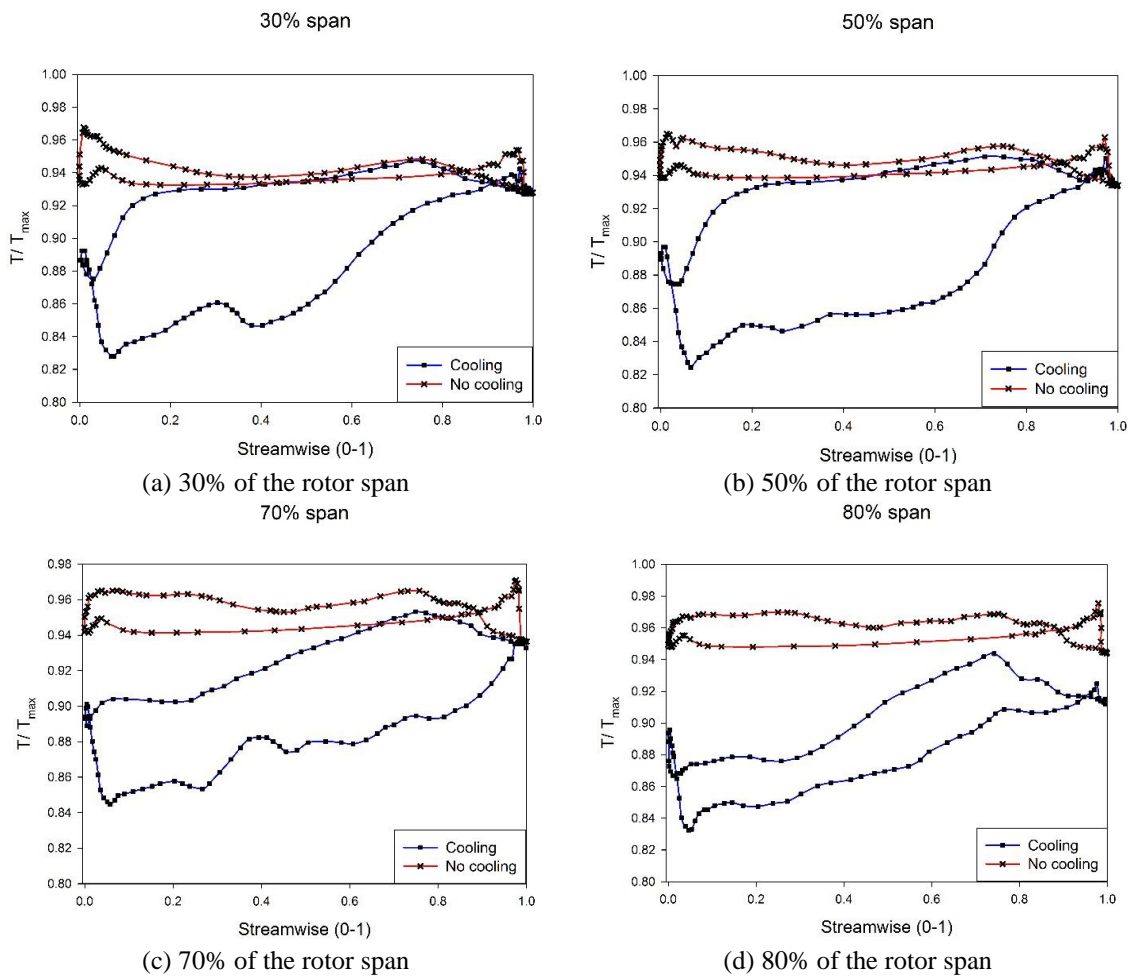
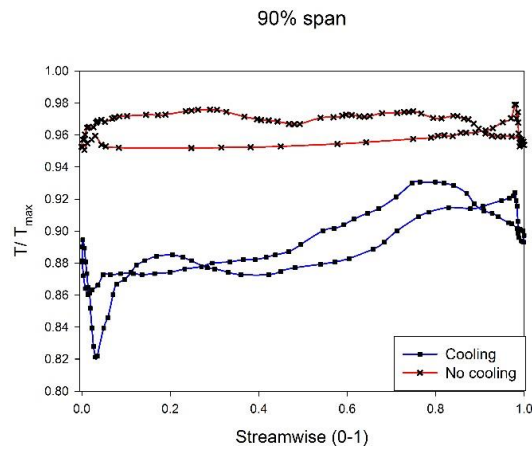


Fig. 8 Rotor temperature comparison for cooling and non-cooling case in different spans



(e) 90% of the rotor span

Fig. 8 Continued

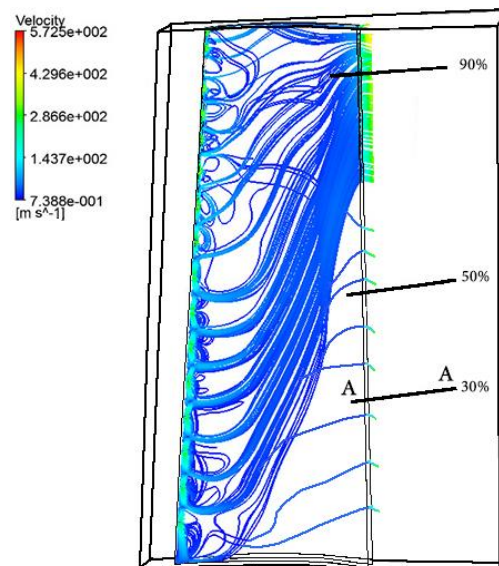


Fig. 9 Coolant streamlines from jets to T.E slot

blade. This mixture reaches the greatest amount of turbulence near the blade tip. This happens because initial jets' flow that is adjacent to the hub tends to leave the blade through the slot, near the tip as near as possible because of rotation effects. Simultaneously, the jets nearby the tip tend to show the same characteristic, but all the flows cannot eject through the trailing edge slot near the tip chronologically so flow mixture in the space between blade and plenum adjoining to the tip is greater and consequently convection heat transfer is more.

4.3 Cooling effects on rotor loss

For the mixture of the coolant with the main flow, loss in blades which are exerted on cooling

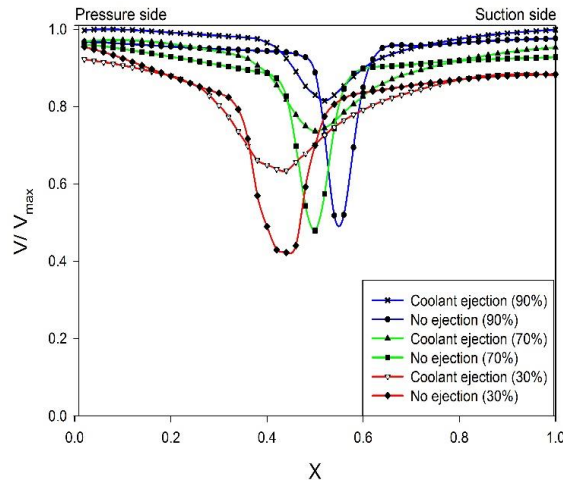


Fig. 10 T.E velocity distribution along line AA in existence of the coolant ejection and no ejection at different spans

technique is more than the non-cooling blades in general. Coolant to main flow velocity ratio, mass flow ratio, slot width and angle of coolant ejection to main flow are factors that impress on the loss, Schobeiri (2012). However investigation on impingement cooling effect on the rotor loss is more complex than nozzle blades. The rotor blade’s trailing edge coolant ejection has a positive effect on losses related to the blade trailing edge wake. Fig. 9 shows the coolant streamline from jet holes to trailing edge ejection to mainstream and their tendency to eject from rotor blade tip for the existence of rotating effects. Fig. 10 shows streamline velocity right after trailing edge in presence and absence of cooling ejection from the slot, along line AA. The line is adjacent of the trailing edge and its length cover trailing edge wakes and main flow streams (X is the dimensionless length of the line AA) seen in Fig. 10 jet impingement coolant ejection at trailing edge impacts the main flow along line AA and its momentum fills the trailing edge wakes. The trailing edge momenta get stronger from hub to tip because of rotation effects and the existence of stronger cooling jets on near the rotor blade’s tip. The maximum speed difference between cooling ejection and non-ejection state along line AA at 30%, 50%, and 90% span is 49.1%, 53.6% and 57.4% respectively, which shows the increase in jets’ ejection speed from trailing edge slot as travelling from hub to tip. (200 samples are used for coolant streamline from jet holes to trailing edge ejection to mainstream in Fig. 9)

5. Conclusions

Numerical solution of the nozzle and the rotor blade showed the jet impingement cooling for the rotor blade in the turbine, increases in local heat transfer. Furthermore, the increase of pressure at the end of the plenum and the addition of the Coriolis and centrifugal effects, cause amplification in jets’ velocity which are located at the end of the plenum so the phenomenon influences on rotor tip heat transfer and causes decrease in the area’s temperature. Moreover, the impingement of coolant ejection through the trailing edge slot, lessens the trailing edge wake effects by sweeping the wakes by increasing the momentum in these regions. These momenta get

stronger at the rotor tip due to the existence of the rotational effects and their declination to leave the blade through trailing edge slot, near the tip.

References

- Bardina, J., Huang, P. and Coakley, T. (1997), "Turbulence modeling validation", *Proceedings of the 28th Fluid Dynamics Conference*, Snowmass Village, Colorado, U.S.A., June-July.
- Bunker, R.S. and Metzger, D.E. (1990), "Local heat transfer in internally cooled turbine airfoil leading edge regions: Part I—impingement cooling without film coolant extraction", *J. Turbomach.*, **112**(3), 451-458. <https://doi.org/10.1115/1.2927680>.
- Chupp, R.E., Helms, H.E., McFadden, P.W. and Brown, T.R. (1969), "Evaluation of internal heat-transfer coefficients for impingement-cooled turbine airfoils", *J. Aircraft*, **6**(3), 203-208. <https://doi.org/10.2514/3.44036>.
- Dong, L.L., Leung, C.W. and Cheung, C.S. (2002), "Heat transfer characteristics of premixed butane/air flame jet impinging on an inclined flat surface", *Heat Mass Transfer*, **39**(1), 19-26. <https://doi.org/10.1007/s00231-001-0288-1>.
- Ekkad, S., Huang, Y. and Han, J.C. (2000), "Impingement heat transfer measurements under an array of inclined jets", *J. Thermophys. Heat Tr.*, **14**(2), 286-288. <https://doi.org/10.2514/2.6524>.
- Froessling, N. (1958), "Evaporation, heat transfer, and velocity distribution in two-dimensional and rotationally symmetrical laminar boundary-layer flow", NACA-TM-14, NACA Technical Memorandum, U.S.A.
- Gau, C. and Chung, C. (1991). "Surface curvature effect on slot-air-jet impingement cooling flow and heat transfer process", *J. Heat Trans.*, **113**(4), 858-864. <https://doi.org/10.1115/1.2911214>.
- Goldstein, R.J. and Cho, H.H. (1995), "A review of mass transfer measurements using naphthalene sublimation", *Exp. Therm. Fluid Sci.*, **10**(4), 416-434. [https://doi.org/10.1016/0894-1777\(94\)00071-F](https://doi.org/10.1016/0894-1777(94)00071-F).
- Greitzer, E.M., Tan, C.S. and Graf, M.B. (2007), *Internal Flow: Concepts and Applications*, Cambridge University Press, Cambridge, U.K.
- Hong, S.K., Lee, D.H. and Cho, H.H. (2008), "Heat/mass transfer measurement on concave surface in rotating jet impingement", *J. Mech. Sci. Technol.*, **22**(10), 1952-1958. <https://doi.org/10.1007/s12206-008-0738-5>.
- Hrycak, P. (1981), "Heat transfer from a row of impinging jets to concave cylindrical surfaces", *Int. J. Heat Mass Tran.*, **24**(3), 407-419. [https://doi.org/10.1016/0017-9310\(81\)90048-X](https://doi.org/10.1016/0017-9310(81)90048-X).
- Hwang, J.J. and Cheng, C.S. (2001), "Impingement cooling in triangular ducts using an array of side-entry wall jets", *Int. J. Heat Mass Tran.*, **44**(5), 1053-1063. [https://doi.org/10.1016/S0017-9310\(00\)00141-1](https://doi.org/10.1016/S0017-9310(00)00141-1).
- Ibrahim, M.B., Kochuparambil, B.J., Ekkad, S.V. and Simon, T.W. (2005), "CFD for jet impingement heat transfer with single jets and arrays", *Proceedings of the ASME Turbo Expo 2005: Power for Land, Sea, and Air*, Reno, Nevada, U.S.A., June.
- Jia, R., Rokni, M. and Sundén, B. (2002), "Numerical assessment of different turbulence models for slot jet impinging on flat and concave surfaces", *Proceedings of the ASME Turbo Expo2002: Power for Land, Sea, and Air*, Amsterdam, The Netherlands, June.
- Li, H.L., Chiang, H.W.D. and Hsu, C.N. (2011), "Jet impingement and forced convection cooling experimental study in rotating turbine blades", *Int. J. Turbo Jet Eng.*, **28**(2), 147-158. <https://doi.org/10.1515/tjj.2011.015>.
- Menter, F.R. (1994), "Two-equation eddy-viscosity turbulence models for engineering applications", *AIAA J.*, **32**(8), 1598-1605. <https://doi.org/10.2514/3.12149>.
- Metzger, D.E. and Rued, K. (1989), "The influence of turbine clearance gap leakage on passage velocity and heat transfer near blade tips: Part I—sink flow effects on blade pressure side", *J. Turbomach.*, **111**(3), 284-292. <https://doi.org/10.1115/1.3262267>.
- Saeed, F. (2008), "Numerical simulation of surface heat transfer from an array of hot-air jets", *J. Aircraft*, **45**(2), 700-714. <https://doi.org/10.2514/1.33489>.

- Schobeiri, M. (2012), *Turbomachinery Flow Physics and Dynamic Performance*, Springer, Berlin, Germany.
- Stevens, J. and Webb, B.W. (1991), "The effect of inclination on local heat transfer under an axisymmetric, free liquid jet", *Int. J. Heat Mass Trans.*, **34**(4-5), 1227-1236. [https://doi.org/10.1016/0017-9310\(91\)90031-9](https://doi.org/10.1016/0017-9310(91)90031-9).
- Tabakoff, W. and Clevenger, W. (1972), "Gas turbine blade heat transfer augmentation by impingement of air jets having various configurations", *J. Eng. Power*, **94**(1), 51-58. <https://doi.org/10.1115/1.3445620>.
- Tu, J., Yeoh, G.H. and Liu, C. (2013), *Computational Fluid Dynamics*, Butterworth-Heinemann, Amsterdam, The Netherlands.